Thin Solid Films 519 (2011) 2698–2702

Contents lists available at ScienceDirect

Thin Solid Films

journal homepage: www.elsevier.com/locate/tsf

Rotatable broadband retarders for far-infrared spectroscopic ellipsometry

T.D. Kang [a,*], E. Standard [a], G.L. Carr [b], T. Zhou [a], M. Kotelyanskii [a,c], A.A. Sirenko [a]

[a] Department of Physics, New Jersey Institute of Technology, Newark, NJ 07102, USA
[b] National Synchrotron Light Source, Brookhaven National Laboratory, Upton, NY 11973, USA
[c] Rudolph Technologies, Inc., Flanders, NJ 07836, USA

ARTICLE INFO

Article history:
Received 22 May 2010
Received in revised form 9 September 2010
Accepted 9 December 2010
Available online 21 December 2010

Keywords:
Far-infrared retarder
Spectroscopic ellipsometry
Rotatable retarder
Total internal reflection
TOPAS
Double-Fresnel rhomb

ABSTRACT

Rotatable retarders have been developed for applications in spectroscopic, full Mueller Matrix ellipsometry in the far-IR spectral range. Several materials, such as silicon, KRS-5, and a commercial polymer plastic (TOPAS) have been utilized to achieve a fully adjustable retardation between 0° and 90°. Experimental characteristics of the rotatable retarders that utilize three- and four-bounce designs are compared with calculations. We discuss the effect of light focusing on the performance of these rotatable retarders.

1. Introduction

Broadband optical retarders are required for spectroscopic ellipsometry in its full Mueller matrix (MM) realization. Performance of the MM ellipsometer depends on the capability to produce substantially linearly-independent Stokes vectors for the light incident onto the sample. As has been shown [1], the errors in the measured MM of the sample are proportional to the condition number of the 4×4 matrix composed of the Stokes vectors of four polarization states incident at the sample. It can be proven that it is impossible to cover the Poincare sphere with linearly-independent Stokes vectors by only changing the linear polarization at the input surface of a stationary retarder. As we will illustrate further in this paper, total coverage of the Poincare sphere is possible by rotating a tandem of a linear polarizer and a retarder with a retardation of 90°. It is this goal that we are trying to achieve in the retarder designs described in this paper.

Traditionally, broadband retarders for the far-IR ellipsometry are made from a single triangular prism where the phase retardation between the *s* and *p* polarizations is achieved by total internal reflection inside the prism. The prism is cut for normal incidence at both the entrance and exit surfaces, thus eliminating any polarization effects at these surfaces. For the internal reflection, the incident angle θ should be greater than the critical angle to avoid intensity losses. By using Fresnel reflection coefficients, the one-bounce retardation δ that occurs from total internal reflection at incident angle θ in a prism material is obtained [2,3]:

$$\tan(\delta/2) = \left(\sin^2\theta - n^{-2}\right)^{1/2} / \left(\sin\theta\,\tan\theta\right) \quad (1)$$

where n is the ratio of refractive indices of the incidence and refraction media, respectively. Calculations for the maximum retardation provided by a single prism made of different materials are shown in Fig. 1(a). Transparent and isotropic materials are typically used, such as Si, KRS-5, polycrystalline ZnSe, or transparent polymer plastics. One can see that a 90° retardation is not always possible with a single reflection, especially for low-index materials, such as TOPAS plastic. However, a 90° retardation can be obtained with two or more internal reflections, such as found in a Fresnel rhomb. The choice of the retarder material is determined by the spectral range of the measurements. For example, the free-carrier absorption at low frequencies and the weak phonon absorption band at 520 cm^{-1} can affect the performance of a Si retarder. KRS-5 can be used only in the frequency range above 400 cm^{-1} due to phonon absorption.

The single-prism (=one internal reflection) retarder design has an obvious disadvantage for the broadband spectroscopic MM

* Corresponding author. Tel.: +1 804 501 6576.
E-mail address: tdkang@njit.edu (T.D. Kang).

0040-6090/$ – see front matter
doi:10.1016/j.tsf.2010.12.057

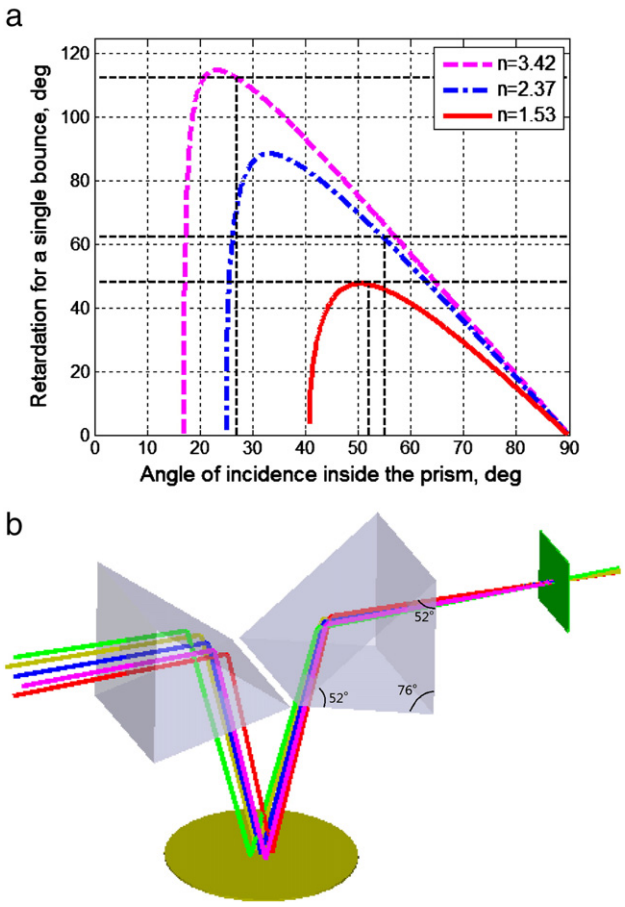

Fig. 1. (a) The relative phase shift between *s* and *p* polarizations for a single bounce at the total internal reflection using far-IR average values of the refractive index of Si: $n=3.42$, KRS-5: $n=2.37$, and TOPAS: $n=1.533$. (b) TOPAS retarder in a focused beam. The central beam that propagates along the optical axis is shown with blue, the 3, 6, 9, and 12 o'clock beams are shown with pink, red, brown, green colors. The sample is shown at the focus point.

ellipsometry. To create at least four linearly-independent Stokes vectors on the sample surface, the retarder should be rotatable, which will ultimately steer the light beam off the optical axis of the ellipsometer. To return the beam back to the optical axis of the ellipsometer, one needs at least two more reflections. However, metal mirrors positioned at a high incident angle are not always suitable for this purpose due to dispersion that would result in a strong spectral dependence of retardation even in the far-IR spectral range. Another problem is related to metal mirror contamination that will also change the retardation over time and will require a frequent recalibration. To avoid this problem, various designs for rotating retarders relying on the double-Fresnel-rhomb approach have been proposed [4,5]. However, no commercial solution is known for the far-IR spectral range.

A far-IR spectroscopic ellipsometer with the full MM capability has been recently developed at the U4IR beamline of the National Synchrotron Light Source (NSLS) at Brookhaven Nat'l Lab (BNL). We investigated the design and performance of retarders made from Si, KRS-5, and TOPAS materials for use in the spectral range between 10 and several thousands of cm^{-1}. Note that TOPAS plastic is transparent in both, visible and far-IR spectral ranges, so this greatly facilitates the procedure for accurately aligning the optical components inside the ellipsometric optical system. This is another reason why TOPAS plastic was chosen, over other common polymer materials for the far-infrared. In this paper, we focus on their performance in the most challenging far-IR spectral range between 10 and 100 cm^{-1}.

Alternatively, birefringent materials could be used as retarders. However, most of the birefringent materials have IR-active optical phonons, so the absorption due to optical phonons will affect their performance in a broad spectral range including the far infrared. Materials, like Si, do not have IR active phonons, but they are not birefringent. Application of external electric field to Si, which can cause birefringence, is not trivial, since it is hard to obtain a uniform field distribution across the large acceptance area of a retarder. Another alternative approach could be based on the application of thin films. However, in this case one can expect a strong dependence of retardation across the optical spectrum. This approach works much better for single wavelength ellipsometry, but in the far-IR the thin-film approach does not seem to be easy.

2. Calculations

One of the designs for the rotating retarder, which has been implemented in our ellipsometer at U4IR beamline at the NSLS, is shown in Fig. 1 (b). It consists of two TOPAS prisms and a gold mirror. A small incidence angle of 14° is used for the mirror reflection, so the possible retardation at the mirror surface is calculated to be ~180° in the far-IR spectral range. Note that, as for the reflection coefficients in this paper, we follow the Nebraska convention [6] by which the Eq. (1) was derived. The refractive index of TOPAS is $n=1.533$ in the far-IR. One bounce results in a ~45° phase shift between *s* and *p* input linear polarizations for the prism angle of about 52°. This angle is marked with a dashed vertical line in Fig. 1(a).

Another design for retarders for the far- and mid-IR spectral range is based on the double-Fresnel rhomb. Fig. 2(a,b) shows the ZEMAX model and pictures of Si retarders. Four internal reflections at the incidence angle of 27° keep the input and the output beams on the optical axis and provide the total phase shift of 450° (360° + 90°). The dashed vertical line in Fig. 1(a) indicates the angle of 27°. Note that if a larger angle of reflection is utilized, so that the total phase shift is 90° or 270°, then the retarder length and, hence, the optical path inside the retarder becomes prohibitively long. A KRS-5 retarder for the mid-IR spectral range has been developed utilizing a four-bounce design yielding a total phase shift of 270°. Its properties will be described elsewhere.

To create a linearly-independent set of the Stokes vectors for the light incident onto the sample, a tandem of a linear polarizer and a retarder is used in the modern ellipsometer design [7]. The MM for the rotating retarder depends on the angle of rotation ϕ with respect to the plane of the input linear polarization. The following expression is a Mueller matrix for the rotated retarder assembly with Δ_C and Ψ_C characterizing the retarder itself [7]:

$$\begin{bmatrix} 1 & \cos2\Psi_c\cos2\phi & \cos2\Psi_c\sin2\phi & 0 \\ \cos2\Psi_c\cos2\phi & \cos^2 2\phi + \sin2\Psi_c\cos\Delta_c\sin^2 2\phi & (1-\sin2\Psi_c\cos\Delta_c)\sin2\phi\cos2\phi & -\sin2\Psi_c\sin\Delta_c\sin2\phi \\ \cos2\Psi_c\sin2\phi & (1-\sin2\Psi_c\cos\Delta_c)\sin2\phi\cos2\phi & \sin2\Psi_c\cos\Delta_c\cos^2 2\beta + \sin^2 2\phi & \sin2\Psi_c\sin\Delta_c\cos2\phi \\ 0 & \sin2\Psi_c\sin\Delta_c\sin2\phi & -\sin2\Psi_c\sin\Delta_c\cos2\phi & \sin2\Psi_c\cos\Delta_c \end{bmatrix}. \quad (2)$$

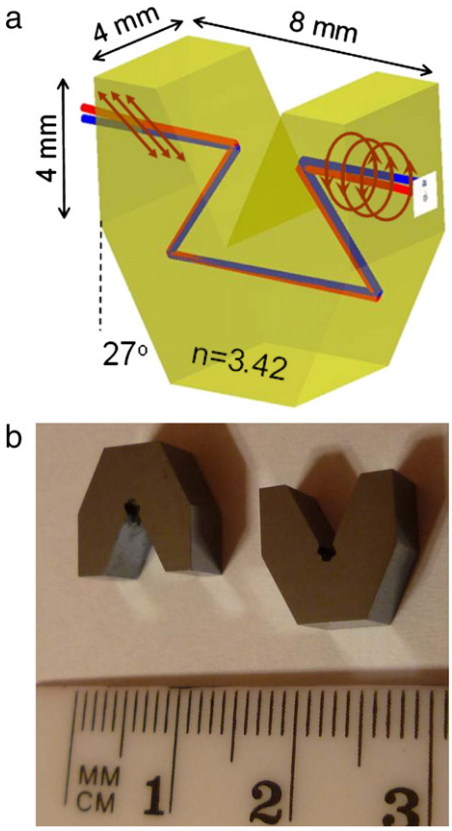

Fig. 2. (a) Design for a silicon double Fresnel rhomb (4 bounces) as a far infrared phase retarder with approximate dimensions shown in the figure. Theoretical operational range is between 10 and 450 cm^{-1}. Polarizations of the incoming and transmitted light are shown schematically for the left and right hand sides of the retarder, respectively. (b) Retarders made of semi-insulating silicon.

Here $\cos \Delta_C = \Delta_F - \Delta_S$ and $\Psi_C = \tan^{-1}(|t_F|/|t_S|)$ are defined with $t_F = |t_F| \exp(i\Delta_F)$ and $t_S = |t_S| \exp(i\Delta_S)$ which are the transmission coefficients along the fast and slow axes, respectively [8].

If the linear polarization changes at the input of an ideal stationary retarder with a quarter-wave retardation ($\Delta_C = 90°$), the corresponding output Stokes vectors form a circle on the plane made of S_1 and S_3 axes on the Poincare sphere. Note that all these Stokes vectors are linearly-dependent, which prevents a full MM analysis of the measured sample. For a tandem of a rotating retarder and a stationary input linear polarizer, the Stokes vectors form a "figure-8"[9], which can produce a number of linearly-independent combinations of the output Stokes vectors. If a full coverage of the Poincare sphere is required, both the input linear polarizer and the retarder need to be rotated. Fig. 3(a) shows results for the output Stokes vectors produced by a 180° rotation of a quarter-wave retarder combined with four different positions of the input linear polarizer.

The maximum value of retardation depends on the prism angle and the refractive index of the prism. Dispersion of the prism material in the far-IR spectral range is not strong, especially in the frequency range below the optical phonon absorption. Nevertheless, dispersion can change the maximum value of retardation at different frequencies. This effect is illustrated in Fig. 3(b) for a retarder configuration as described in Fig. 1(b), which shows results of calculation for the same prism and three values of the refractive index: $n = 1.4$, $n = 1.7$, and $n = 1.533$, where the latter is the known value for TOPAS in the far-IR, and $n = 1.4$, and $n = 1.7$ are chosen for illustration purpose. Here, we assumed 180° of the retardation from the mirror reflection. One can see that in the lower-index cases, there is an "undershoot" around the poles of the Poincare sphere, and in the higher-index case, there is an "overshoot". Both the higher-index and the lower-index cases would leave a "hole" around the pole preventing a complete coverage of the Poincare sphere.

In a real ellipsometer, the light is usually focused on a sample and the retarder should be placed in a cone of the focused light [Fig. 1(b)]. To minimize the polarization variation across the light beam, usually a slow focusing is chosen with the f-number more than 20. In our ellipsometer at U4IR beamline $f = 40$, which gives the beam convergence of about $\pm 1.43°$. Nevertheless, the retarders produce a change of polarization across the beam profile. Five beams were analyzed: "3", "6", "9", and "12 o'clock" including the reference beam that passes along the optical axis and is marked with "zero". The absolute values of the angles between the Stokes vectors that correspond to the central beam and the other four beams are shown in Fig. 4 for the TOPAS retarder. For each focused beam these values oscillate between zero and 2.3° for the complete rotation of the retarder. This corresponds to the variation in the individual components of the generated Stokes vectors δS not exceeding $\tan(2.3°) \approx 0.04$.

The four-bounce Si retarder [Fig. 2(a)] turns out to be less sensitive to the focusing effects. For the same $f = 40$, the focused beams inclined in the vertical plane ("6" and "12 o'clock") do not change the state of polarization in the first order approximation due to the self-correction provided by the four-bounce design. It is evident from the retardation curve for Si prism in Fig. 1(a). As long as the "working point" for Si (27°) is on the linear slope of the curve, the total retardation after four internal bounces is not affected by the focusing. This simple argument has been confirmed by ZEMAX calculations. In the horizontal plane the maximum deviation of the Stokes vector across the beam is 1.8°, which corresponds to $\delta S = 0.032$. It means that if the 45° linearly polarized light with $S_{in} = [1\,0\,1\,0]^T$ is focused on the retarder, the "zero", "6", and "12 o'clock" beams after the Si retarder will be circularly polarized with $S_{out} = t[1\,0\,0\,1]^T$, while the "3" and "9 o'clock" beams will exit with the state of polarization in the range $S_{out} = t[1 \pm 0.032\,0\,0.9995]^T$. Here t is the transmission coefficient. The complete effect of the focusing systematic error on the accuracy of the Mueller matrix measurement requires a more detailed analysis of the entire ellipsometer system including the intensity distribution across the focused beam, and it also depends on the sample properties.

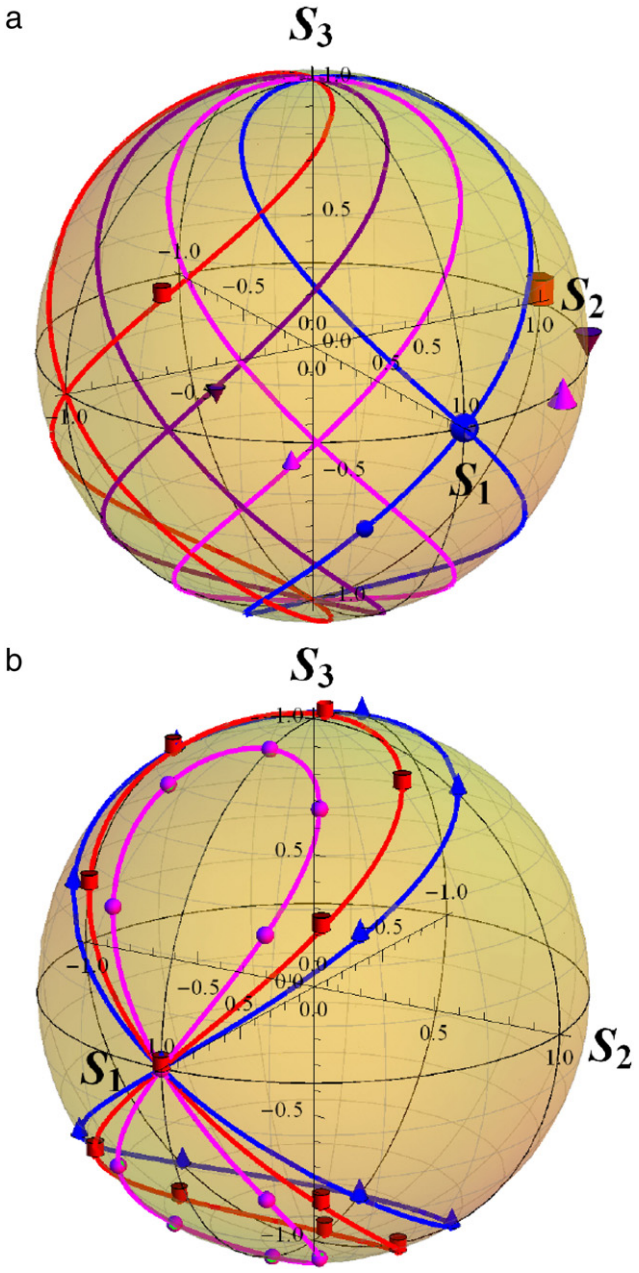

Fig. 3. (a) Polarization states on the Poincare sphere for four positions of the input linear polarizer: 0°(blue), 15°(magenta), 30°(purple), and 45°(red). Note that a uniform coverage of the sphere is possible for rotation of the input linear polarizer. (b) The Poincare sphere for polarization changes for a rotating retarder made of two prisms with a fixed angle of 52° and three different values of the refractive index: $n=1.4$ (magenta), $n=1.533$ (red), and $n=1.7$ (blue).

3. Experimental results

Experimental calibrations for a double-prism TOPAS and Si retarders were carried out at the U4IR beamline at NSLS-BNL. The experimental setup is composed of three wire-grid linear polarizers (P_0, P_1, A) and a single retarder (C) positioned in the following order: P_0, P_1, C, and A, respectively. The behavior of the TOPAS retarder used in our experiments is the following: linearly-polarized radiation (after the wire-grid polarizer) enters the retarder front surface, which is normal to the beam direction. After the total internal reflection, the beam is directed to the gold mirror. The maximum value of the phase shift after the first internal reflection is ~45°. The small incident angle for the gold reflection results in a negligible change in the retardation.

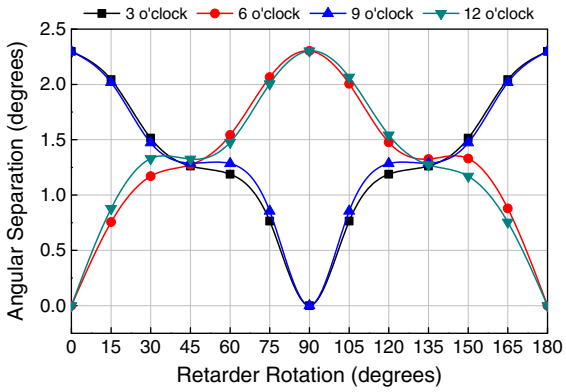

Fig. 4. The angle separation between the Stokes vectors for the central beam and four focused beams propagating at 3, 6, 9, and 12 o'clock through the prism retarder as shown in Fig. 1(b).

After passing the second prism, the beam is acquiring the total phase shift of up to ~90°. The kinematic mount of the small gold mirror provides the opportunity for the beam alignment inside the retarder assembly and enables the straight light propagation through the retarder.

Polarization of the transmitted light was analyzed in the rotating analyzer configuration for multiple positions of the retarder angle with respect to a fixed value of the P_0 and P_1 polarizers. We put P_1 parallel to P_0 in order to optimize the linear polarization of the incident beam, and set them to 45°. As shown in Fig. 5(a) and (b), we present the tan Ψ and cos Δ values on the TOPAS and Si retarders at the wave number of ~60 cm^{-1} as functions of angular position of the retarders, and their fits with theoretical values described as follows. By using Eq. (2) and assuming the ideal polarizers, we can obtain the theoretical tan Ψ and cos Δ when $P_0=P_1=45°$.

$$\tan\Psi = \sqrt{\frac{(-2-2\cos2\Psi_C(\cos2\phi' + \sin2\phi') - \sin4\phi'(1-\cos\Delta_C\sin2\Psi_C))}{(-2+2\cos2\Psi_C(\cos2\phi' - \sin2\phi') + \sin4\phi'(1-\cos\Delta_C\sin2\Psi_C))}}, \quad (3)$$

$$\cos\Delta = \frac{\cos\Delta_C\cos^2 2\phi'\sin2\Psi_C + \cos2\Psi_C\sin2\phi' + \sin^2 2\phi'}{(1+\cos2\Psi_C\sin2\phi')\sqrt{1-\frac{\cos^2 2\phi'\left(\cos2\Psi_C + (1-\cos\Delta_C\sin2\Psi_C)\sin^2 2\phi'\right)^2}{\left(1+\cos2\Psi_C\sin2\phi'\right)^2}}}, \quad (4)$$

where $\phi'=\phi-\phi_0$, the practical angle of the fast axis relative to the zero which is determined by referring to the azimuth angles of the linear polarization of the incident beam and which is off by ϕ_0 from the measured angular position ϕ. As shown in Table 1, we obtained the values of tan Ψ_C (Ψ_C), cos Δ_C (Δ_C), and ϕ_0 as well as their error bars with a confidence level of 95% for the TOPAS and Si retarders by fitting the measured tan Ψ and cos Δ simultaneously with Eqs. (3) and (4), respectively. In this calculation, the experimental values for the attenuation ratio of the linear polarizers, which was measured to be less than 0.01 between 15 and 100 cm^{-1}, produce an insignificant correction. For example, by using formulas for the rotating analyzer configuration with imperfect polarizers [10], the possible changes of Δ_C by 0.01 of the attenuation ratio are estimated to be about 0.1° for the TOPAS retarder and 0.2° for the Si retarder, which are less than the error bars of Δ_C. The tan Ψ_C values for the TOPAS and Si retarders were estimated to be 0.997 and 0.980, respectively, which can be ideal (tan $\Psi_C=1$) within their error bars. However, such tan $\Psi_C\neq1$ does not affect the accuracy of the measurement of Mueller matrix as long as we know the exact Ψ_C values. The 84.66° and 80.27° for the maximum retardations, Δ_C, of the TOPAS and Si retarders are close to 90°, which we expected to obtain.

Fig. 5(c) and (d) shows tan Ψ and cos Δ for $\phi=0°$, for which the experimental values of retardation can be obtained closest to 90° in

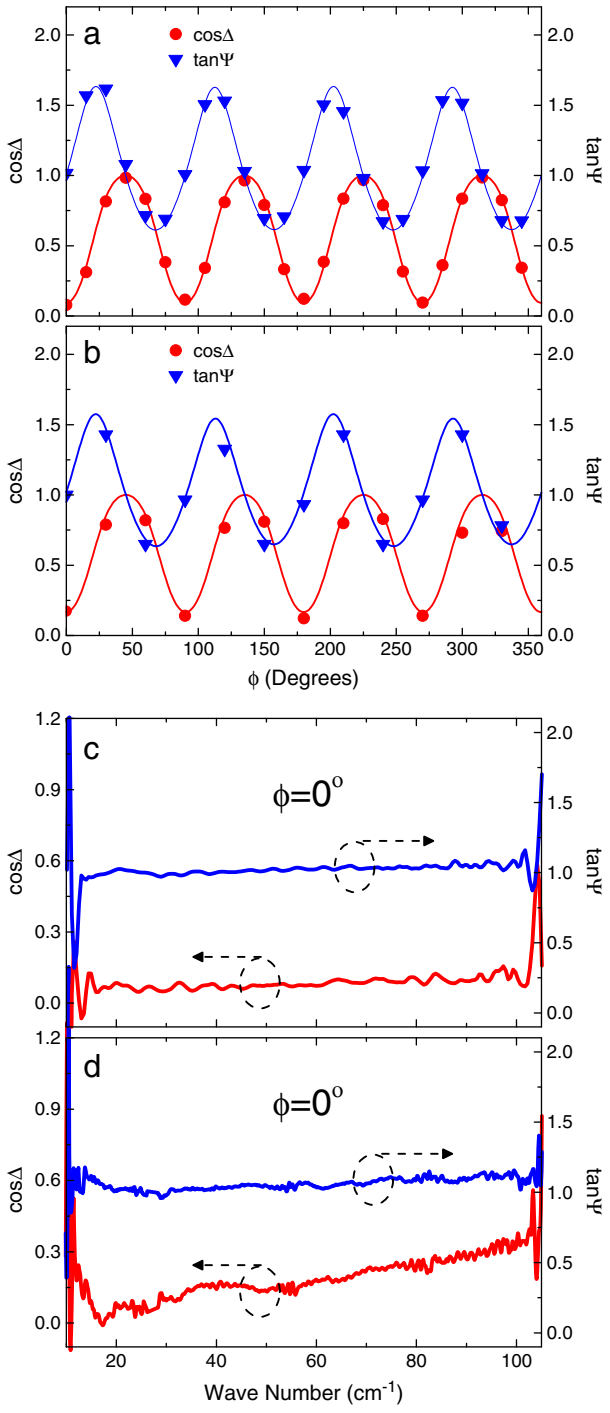

Fig. 5. Experimental data (circles and triangles) and fit results (solid curves) for cos Δ and tan Ψ as a function of the rotation angle ϕ for (a) TOPAS and (b) Si retarders. Spectral dependencies of cos Δ and tan Ψ for (c) TOPAS and (d) Si retarder for $\phi = 0°$.

the frequency range which is determined by the sensitivity of our bolometer: 15 cm^{-1}–100 cm^{-1}. The wiggling feature in the data for the TOPAS retarder [Fig. 5(c)] is attributed to the contribution from the imperfection of optics such as the depolarization at the surfaces of the TOPAS prisms, and the polarization sensitivity of the detector. Even with a straight-through rotating analyzer ellipsometry (RAE) configuration without retarders, we observed a similar sinusoidal pattern with a period of ~15 cm^{-1} in the measured tan Ψ and cos Δ,

Table 1
Parameters for TOPAS and silicon retarders estimated from the measured tan Ψ and cos Δ.

	TOPAS retarder		silicon retarder	
	value	error bar	value	error bar
Ψ_C	44.90°	±0.27°	44.41°	±0.81°
tan Ψ_C	0.997	±0.009	0.980	±0.028
Δ_C	84.66°	±0.53°	80.27°	±1.42°
cos Δ_C	0.093	±0.009	0.169	±0.024
ϕ_0	−0.1°	±0.2°	0.1°	±0.7°

thus confirming that these artifacts originate from the polarization sensitivity of the detector. As for the data on the Si retarder shown in Fig. 5(d), the relatively sharp and fast features at around 27, 53, and 80 cm^{-1} are interference patterns caused by the beam splitter in the Fourier Transform Infrared (FTIR) spectrometer.

At lower wave numbers, diffraction losses and the decrease in the synchrotron source intensity make the use of a small TOPAS retarder difficult. Though a larger retarder could improve the low-frequency performance, absorption inside the TOPAS results in a decreasing transmission. The overall intensity attenuation for a single TOPAS retarder is significant and wavelength-dependent. It is mostly determined by absorption from the long optical path inside the prism material. For example, the retarder with a 15 mm acceptance aperture has the attenuation ratios of 1:10 at 20 cm^{-1} and 1:120 at 85 cm^{-1}. A retarder with a reduced size and twice smaller acceptance aperture of 7.5 mm results in the attenuation ratios of 1:4 at 25 cm^{-1} and 1:12 at 85 cm^{-1}. In spite of the significant attenuation factor, the reserves of the synchrotron radiation intensity make the application of these types of retarders possible for far-IR ellipsometry.

4. Conclusion

To realize a full-Mueller-matrix spectroscopic ellipsometer in the IR spectral range, rotatable broadband retarders made of TOPAS plastic, Si, and KRS-5 were designed and developed based on their known or measured refractive index. The retarders made of the TOPAS plastic and Si were characterized using the rotating analyzer ellipsometry in the far-IR spectral range between 10 and 105 cm^{-1}. We estimated the characteristics of the retarders by comparing with the theoretical calculation, and observed them working in the spectral range along with their rotations.

Acknowledgements

This work is supported by NSF-MRI-0821224 at NJIT and by the U. S. DOE under contract DE-AC02-98CH10886 at the NSLS.

References

[1] A. De Martino, E. Garcia-Caurel, B. Laude, B. Drévillon, Thin Solid Films 455–456 (2004) 112.
[2] R.M.A. Azzam, N.M. Bashara, Ellipsometry and Polarized Light, Elsevier Science, New York, 1987.
[3] M. Born, E. Wolf, Principles of Optics, 6th ed., Pergamon Press Inc., Elmsford, New York, 1980, p. 50.
[4] J. den Boer, Spectroscopic Infrared Ellipsometry: Components, Calibration, and Application, Eindhoven University of Technology, Eindhoven, 1995, p. 62.
[5] N.N. Nagib, S.A. Khodier, Appl. Opt. 34 (1995) 2927.
[6] R.H. Muller, Surf. Sci. 16 (1969) 14.
[7] P.S. Hauge, J. Opt. Soc. Am. 68 (1978) 1519.
[8] H.G. Tompkins, E.A. Irene, Handbook of Ellipsometry, William Andrew Publishing, Inc., Norwich, New York, 2005.
[9] R.M.A. Azzam, J. Opt. Soc. Am. A 17 (2000) 2105.
[10] M. Luttemann, J.-L. Stehle, C. Defranoux, J.-P. Piel, Thin Solid Films 313–314 (1998) 631.